Multiscale Coarse Graining of Diblock Copolymer Self-Assembly: From Monomers to Ordered Micelles

Carlo Pierleoni,[1] Chris Addison,[2] Jean-Pierre Hansen,[2] and Vincent Krakoviack[3]
[1]INFM CRS-SOFT, and Department of Physics, University of L'Aquila, I-67010 L'Aquila, Italy
[2]Department of Chemistry, University of Cambridge, Cambridge CB2 1EW, United Kingdom
[3]Laboratoire de Chimie, Ecole Normale Supérieure de Lyon, 69364 Lyon Cedex 07, France
(Received 18 January 2006; published 31 March 2006)

Starting from a microscopic lattice model, we investigate clustering, micellization, and micelle ordering in semidilute solutions of AB diblock copolymers in a selective solvent. To bridge the gap in length scales, from monomers to ordered micellar structures, we implement a two-step coarse-graining strategy, whereby the AB copolymers are mapped onto ultrasoft dumbells with monomer-averaged effective interactions between the centers of mass of the blocks. Monte Carlo simulations of this coarse-grained model yield clear-cut evidence for self-assembly into micelles with a mean aggregation number $n \simeq 100$ beyond a critical concentration. At a slightly higher concentration the micelles spontaneously undergo a disorder-order transition to a cubic phase. We determine the effective potential between these micelles from first principles.

DOI: 10.1103/PhysRevLett.96.128302 PACS numbers: 82.35.Jk, 61.20.Ja, 64.60.Cn

Block copolymers in solution show a remarkable tendency to self-assemble into a bewildering range of disordered (liquidlike) and ordered structures, depending on the macromolecular composition, the relative sizes of the blocks, solvent selectivity, polymer concentration, and temperature [1,2]. Complex phase diagrams of styrene-isoprene diblock copolymers in various solvents have been mapped out experimentally in great detail by varying the above physical parameters, using a combination of light scattering, small-angle neutron and x-ray scattering, and rheological studies [3,4]. A frequent, partial scenario sees the copolymers aggregate into polydisperse spherical micelles at low polymer concentration; upon lowering the temperature or increasing the concentration, the micelles undergo a disorder-order transition onto a cubic lattice. A theoretical understanding of copolymer phase behavior generally relies on phenomenological considerations [5], or on self-consistent field theory similar to that applied earlier to copolymer melts [6]. A more molecular approach is obviously very difficult, in view of the wide range of length scales involved, from the monomer level to the mesoscopic scales characterizing ordered micellar structures. In particular, monomer-level Monte Carlo (MC) simulations have so far been restricted to short copolymer chains [7].

In this Letter we propose and implement a two-stage coarse-graining strategy to investigate the micellization and disorder-order transition of a simple microscopic model of diblock copolymers. The AB copolymers are made up of two blocks of equal numbers $M_A = M_B = M$ of monomers on a cubic lattice. N such chains occupy a fraction of the lattice sites. The remaining sites are occupied by an implicit solvent chosen to be selective (good solvent) for the B blocks, while it is a θ solvent for the A blocks. This situation is crudely represented by modelling the A blocks as ideal chains (I) and the B blocks as self and mutually avoiding walks (S). Moreover A and B blocks of the same or different copolymers are assumed to be mutually avoiding (S). The resulting model will be referred to as ISS. The model is clearly athermal, so that temperature will be irrelevant, and the polymer density $\rho = N/L^3$ is the only thermodynamic variable (L^3 being the total number of sites of the cubic lattice, the spacing a of which will be taken as the unit of length). With typical polymer sizes $M \simeq 10^3$, and expected micelle aggregation numbers $n \simeq 10^2$, very large system sizes would be needed to generate the tens of micelles required to study their ordered and disordered structures.

The first stage of our coarse-graining procedure, designed to overcome the above bottleneck, is inspired by earlier work on homopolymers [8,9]. AB copolymers are mapped onto ''ultrasoft'' asymmetric dumbells with effective interactions $v_{\alpha\beta}(R)$ between the centers of mass (c.m.) of A and B blocks on different copolymers, and an intramolecular ''tethering'' potential $\phi_{AB}(R)$ between the c.m.'s of the two blocks of the same copolymer [10]. Since the original model is athermal, these effective interactions are purely entropic and are determined by taking statistical averages over copolymer conformations for fixed A-A, A-B, and B-B c.m. distances R. In practice this is achieved by inverting the c.m.-c.m. intermolecular and intramolecular pair distribution functions $g_{AA}(R)$, $g_{AB}(R)$, $g_{BB}(R)$, and $s_{AB}(R)$. The inversion was carried out in the low density limit, using pair distribution functions generated in monomer-level MC simulations of two diblock copolymers with $2M = 500$ monomers each, and an exact relation between the $g_{\alpha\beta}(R)$, $s_{AB}(R)$ and the corresponding $v_{\alpha\beta}(R)$, $\phi_{AB}(R)$ [10]. The resulting pair potentials are shown in Fig. 1, where they are compared to the corresponding pair potentials for an equimolar binary mixture of untethered A and B homopolymers; in the latter case the inversion procedure is trivial in the zero density limit

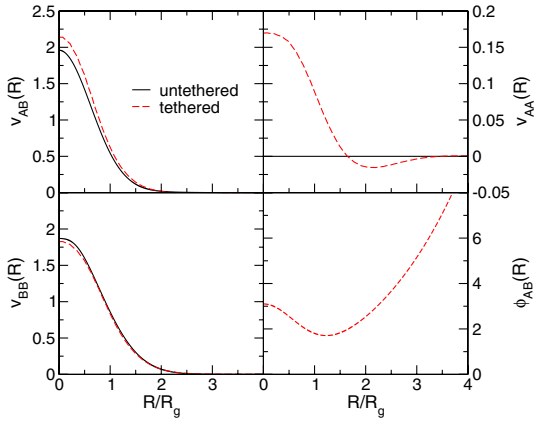

FIG. 1 (color online). Effective pair potentials $v_{AA}(R)$, $v_{AB}(R)$, $v_{BB}(R)$, and $\phi_{AB}(R)$ for tethered and untethered block copolymers in the zero density limit.

where the effective potentials $v_{\alpha\beta}(R)$ and $\phi_{AB}(R)$ reduce to the potentials of mean force, e.g., $v_{\alpha\beta}(R) = -k_BT \ln g_{\alpha\beta}(R)$. The two sets of effective pair potentials $v_{AB}(R)$ and $v_{BB}(R)$ are seen to be surprisingly close. As in the case of homopolymers [8,9] they are roughly Gaussian in shape with an amplitude of a few k_BT, and a range of the order of the radius of gyration R_g of the copolymer. In lattice units, the MC simulations yield the following radii for an isolated copolymer with $2M = 500$: $R_{g,A} = 6.964$, $R_{g,B} = 11.274$, $R_g = 13.889$, while the root mean square distance between the c.m.'s of the two blocks is $R_{AB} = 20.661$. The results for $v_{AB}(R)$ and $v_{BB}(R)$ in Fig. 1 suggest that tethering of the two blocks does not significantly modify their effective interactions. This is no longer true for $v_{AA}(R)$, since this potential is strictly zero in the untethered (binary mixture) case, while it is about 10% of $v_{BB}(R)$ for the copolymer; this residual effective interaction between the ideal blocks is induced by the tethering to nonideal B blocks.

The key assumption made in this work is that these zero density pair potentials are transferrable to finite copolymer densities; i.e., we neglect the density dependence of the effective potentials. Earlier experience with homopolymers shows that this is not an unreasonable approximation well into the semidilute regime $\rho/\rho^* \lesssim 5$ where $\rho^* = (4\pi R_g^3/3)^{-1}$ is the overlap density [9].

We have carried out extensive MC simulations of samples of 5×10^3 and 10^4 AB copolymers using the effective pair potentials of Fig. 1, in the range $3 \leq \rho/\rho^* \leq 10$. The simulations using the coarse-grained representation are at least 2 orders of magnitude faster than simulations of the original all-monomer lattice model. This has allowed us to make detailed investigations, using both sets of potentials in Fig. 1, in order to ascertain the sensitivity of the micellization behavior to details of the effective pair potentials. Both sets of potentials yield results in semiquantitative agreement, and only those obtained with the untethered potentials will be shown here. Inspection of snapshots of configurations shows that micellization sets in between $\rho/\rho^* = 4$ and $\rho/\rho^* = 5$, with the ideal A blocks forming the dense core, as one might expect because of the low or vanishing energy penalty, while the B blocks form the corona, where their energetically unfavorable overlap is minimized. The critical micellar concentration (CMC) observed with our model is quite high compared to most experimentally observed CMC's. This is due to the athermal nature of our simple AB copolymer model, which ignores enthalpic contributions that would drive micellization at much lower concentrations. An unambiguous definition of a micelle remains somewhat arbitrary because of the size polydispersity, but we used the operational convention that all A blocks whose centers are situated within a distance r_c of any other A block belong to the same cluster. The resulting distributions $P(n)$ of aggregation numbers n are shown in panel a of Fig. 2 for $\rho/\rho^* = 3$, 5, and 6, based on a cutoff distance $r_c = 0.8R_g$. $P(n)$ turns out to be very sensitive to the precise value of r_c for $\rho/\rho^* \leq 4$ but nearly independent of the cutoff at higher densities, suggesting that well-defined micelles appear only beyond an estimated CMC of $\rho/\rho^* \sim 5$. At that concentration $P(n)$ exhibits a broad peak around $n \simeq 70$, which narrows and shifts to a mean aggregation number $n \simeq 100$ for $\rho/\rho^* \gtrsim 6$. Figure 2(b) shows the corresponding distribution $P(R_c)$ of the cluster radii (R_c) defined as

$$R_c^2 = \frac{1}{n}\sum_{i=1}^{n} |\vec{R}_i^A - \vec{R}_{\text{c.m.}}|^2 \qquad (1)$$

where $\vec{R}_i^A$ is the position of the ith A block belonging to an n cluster and $\vec{R}_{\text{c.m.}}$ the position of the instantaneous c.m. of that cluster. At $\rho/\rho^* = 3$, $P(R_c)$ is seen to peak at a low value of R_c corresponding to small clusters; the distribution becomes bimodal at $\rho/\rho^* = 5$, signalling the prox-

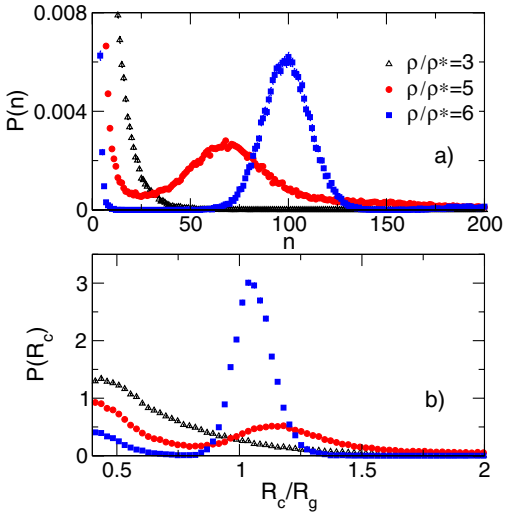

FIG. 2 (color online). (a) Probability of a cluster of n monomers. (b) Probability distribution of the cluster radius R_c.

imity of the CMC, while at $\rho/\rho^* = 6$, $P(R_c)$ shows a sharp peak around $R_c \simeq R_g$, corresponding to micelles of well-defined core size. The peak sharpens and moves to lower values of R_c at still larger values of ρ/ρ^*, indicative of a contraction of the core with copolymer concentration. The internal structure of the micelles is best characterized by the density profiles $\rho_A(R)$ and $\rho_B(R)$ of the centers of A and B blocks around the micelle c.m. The profiles shown in Fig. 3 for $\rho/\rho^* = 7$ are averaged over all micelles formed during the MC simulations, i.e., over size polydispersity. As expected, $\rho_A(R)$ peaks at the origin and drops rapidly to zero for $R > R_g$, while the profile $\rho_B(R)$ practically vanishes for $r < R_g$ and peaks at $R \simeq 2R_g$, thus defining the corona radius. The sharp distinction between micelle core and corona evident from profiles at $\rho/\rho^* = 7$ gradually blurs as the copolymer concentration decreases, thus signalling that the micelles dissolve into a quasihomogeneous solution of copolymers.

A periodic sample of 5000 AB copolymers generated about 50 micelles, and the second step of our coarse-graining procedure is to consider the structure of the system of micelles, regarded as well-defined spherical colloids. Figure 4 shows the pair distribution function $g_m(R)$ of the c.m.'s of the micelles, extracted from the MC simulations for copolymers concentrations $\rho/\rho^* = 5$, 5.5, and 6. All $g_m(R)$ go rapidly to zero for $R < 4R_g$, indicative of a strong effective short-range repulsion between micelles. The structure at $\rho/\rho^* = 5$ is typical of that of a dense colloidal fluid, but it is considerably enhanced at $\rho/\rho^* = 6$, with the amplitude of the main peak jumping from 1.7 (at $\rho/\rho^* = 5$) to over 3 while the split second peak in $g_m(R)$ is characteristic of a cubic structure. The sudden change in pair structure is suggestive of a disorder-order transition, and snapshots of micelle configurations, shown in Fig. 4, confirm this interpretation. Note that at $\rho/\rho^* = 6$, an initially disordered micelle configuration evolves spontaneously to the defective ordered structure shown in Fig. 4 after few tens of thousands MC cycles. More work is under way to determine the symmetry of the observed structure by computing the structure factor $S(q)$. Since the number of micelles generated in the simulations does not, in general, match the "magic number" of particles in the simulation cell compatible with a given crystal structure and periodic boundary conditions, the observed ordered phase is necessarily distorted, but this problem will be alleviated by simulating larger systems, which is possible within our coarse-graining scheme.

From the MC generated pair distribution function $g_m(R)$ at $\rho/\rho^* = 5$ one can extract an effective micelle-micelle pair potential using the hypernetted chain (HNC) integral equation of liquid state theory [11], according to

$$v_m(R) = k_B T\{g_m(R) - 1 - c_m(R) - \ln[g_m(R)]\}, \quad (2)$$

where the direct correlation function $c_m(R)$ is related to $g_m(R)$ by the Ornstein-Zernike relation [11]. The resulting effective pair potential shown in Fig. 4 exhibits a relatively soft repulsion, which culminates at a finite value at $r = 0$, followed by a shallow attractive well. Assuming a Gaussian-like core, a fit to the data in the range $0.5 \leq r \leq 3.5$ provides $v_m(0) \simeq 12k_B T$. The accuracy of the inversion procedure is vindicated by a direct MC simulation of micelles (represented as point particles) interacting via

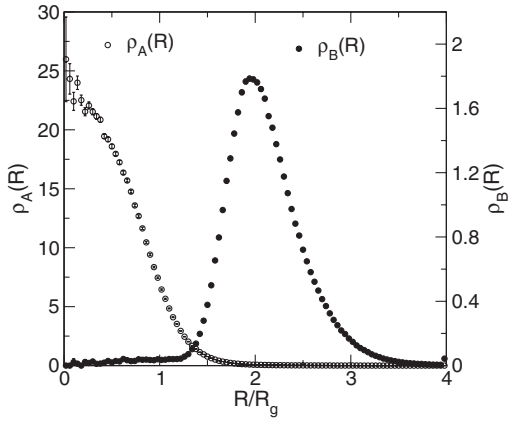

FIG. 3. $\rho/\rho^* = 7$. Density profiles of A blocks (open symbols) and B blocks (closed symbols) with respect to the c.m. of each cluster averaged over all clusters with $n \geq 40$. Note the different scales for ρ_A (left axis) and ρ_B (right axis).

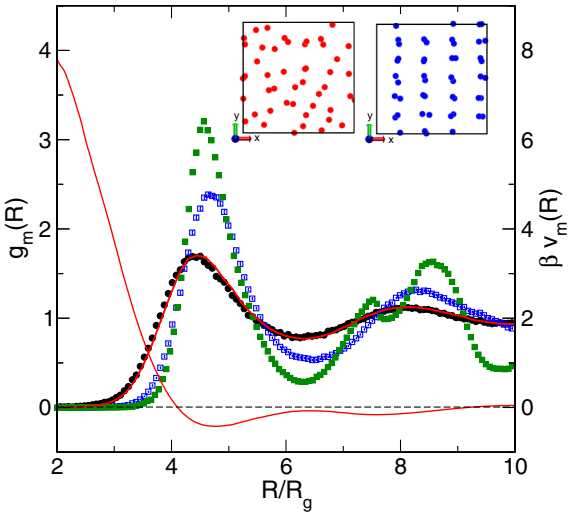

FIG. 4 (color online). Pair distribution function $g_m(R)$ of the c.m.'s of the micelles at $\rho/\rho^* = 5$ (closed circles), 5.5 (open squares), and 6 (closed squares). The HNC potential $v_m(R)$ at $\rho/\rho^* = 5$ is shown by a continuous line (in red online). The corresponding pair correlation is shown as a thick curve in very good agreement with $g_m(R)$ at $\rho/\rho^* = 5$. The potential scale is on the right axis and the value of the potential at the origin is roughly $12k_B T$ (out of scale). Finally, the snapshots in the upper part of the figure show the x-y plane projection of the position of the center of mass of the micelles in a typical configuration at $\rho/\rho^* = 5$ (left-disordered) and 6 (right-ordered).

this $v_m(R)$: the resulting pair distribution functions, also shown in Fig. 4, are indistinguishable from the $g_m(R)$ generated in the original simulation of the underlying copolymer system, signalling the success of the second step in our hierarchical coarse-graining procedure. Potentials like $v_m(R)$ shown in Fig. 4, which remain finite as $R \to 0$, can give rise to a freezing transition at sufficiently high densities, as shown, e.g., in the case of the Gaussian core potential [12,13]. The effective potential is softer than often assumed, but sufficiently repulsive to prevent micelle overlap. It differs significantly from the logarithmic star polymer potential sometimes used to analyze experimental structure factor data [14], because the micelle cores of our model are partly swollen, reflecting the ideal nature of the A blocks. The predicted weak attractive tail is reminiscent of the attractive interaction sometimes assumed to explain or fit measured intermicellar structure factors [14,15]. In view of the effective, purely entropic nature of the potential shown in Fig. 4, it is difficult to give a simple physical picture of its origin; it reflects the tendency of micelles to aggregate into ordered structures. The overall scenario described above is also observed when the low density effective potentials $v_{\alpha\beta}(R)$ for the tethered AB copolymer are used (cf. Figure 1), except that the CMC and disorder-order transition are shifted to higher densities ($\rho/\rho^* \simeq 6$ and 7, respectively). Moreover, the A-block density profiles (similar to those shown in Fig. 3), now develop a minimum at $R = 0$ at higher densities, so that the micelles tend to become "hollow" and increase in size. This is easily understood from the weak short-range repulsion in $v_{AA}(R)$ shown in Fig. 1.

In summary, we have developed a two-step coarse-graining procedure for the description of self-assembly and micelle ordering of diblock copolymers in a selective solvent. The proposed method has been validated for a highly simplified, athermal AB copolymer model. While the phase behavior observed for this model is in qualitative agreement with experimental observations, it would need some straightforward refinement to be more realistic. In particular, an attractive energy $-\epsilon$ between adjacent A monomers [16] would allow the solvent selectivity to be varied and to introduce temperature effects, in particular, the critical micellar temperature [1–4]. In most experimental situations micellization is driven by A-block micro-segregation below their θ temperature, which leads to more compact cores than those observed for our model, and would prevent the spurious artifact of hollow micelles observed in some of our simulations. Enthalpic effects would also lead to a much richer phase diagram upon varying concentration, temperature, as well as the length ratio f, of the two strands. In particular, the model could be tuned to vary the symmetry of the ordered phase and induce, e.g., the bcc-fcc transition observed in many copolymer solutions [17]. Work along these lines is in progress.

C. A. wishes to thank the EPSRC for financial support. Part of this work was carried out while C. P. was at Cambridge, and he wishes to thank Schlumberger for its support. The authors are grateful to A. A. Louis for useful discussions.

[1] T. P. Lodge, J. Bang, Z. Li, M. H. Hillinger, and Y. Talmon, Faraday Discuss. **128**, 1 (2005), as well as subsequent papers published in those Proceedings.
[2] A useful compilation of experimental and theoretical papers on block copolymer self-assembly is contained in I. W. Hamley, *Block Copolymers in Solution* (Wiley, Chichester, 2005).
[3] T. P. Lodge, B. Pudil, and K. J. Hanley, Macromolecules **35**, 4707 (2002).
[4] M. J. Park, K. Char, J. Bang, and T. P. Lodge, Macromolecules **38**, 2449 (2005).
[5] For a recent example see E. B. Zhulina, M. Adam, J. La Rue, S. S. Sheiko, and M. Rubinstein, Macromolecules **38**, 5330 (2005).
[6] L. Leibler, Macromolecules **13**, 1602 (1980); G. H. Frederickson and E. Helfand, J. Chem. Phys. **87**, 697 (1987); M. W. Matsen and M. Schick, Phys. Rev. Lett. **72**, 2660 (1994).
[7] See, e.g., A. Milchev, A. Bhattacharya, and K. Binder, Macromolecules **34**, 1881 (2001); Y. Termonia, J. Polym. Sci., Part B: Polym. Phys. **40**, 890 (2002).
[8] J. Dautenhahn and C. K. Hall, Macromolecules **27**, 5399 (1994).
[9] P. G. Bolhuis, A. A. Louis, J. P. Hansen, and E. J. Meijer, J. Chem. Phys. **114**, 4296 (2001).
[10] C. I. Addison, J. P. Hansen, V. Krakoviack, and A. A. Louis, Mol. Phys. **103**, 3045 (2005).
[11] See, e.g., J. P. Hansen and I. R. McDonald, *Theory of Simple Liquids* (Academic Press, London, 1986), 2nd ed.
[12] F. H. Stillinger and D. K. Stillinger, Physica (Amsterdam) **244A**, 358 (1997).
[13] A. Lang, C. N. Likos, M. Watzlawek, and H. Löwen, J. Phys. Condens. Matter **12**, 5087 (2000).
[14] M. Laurati, J. Stellbrink, R. Lund, L. Willner, D. Richter, and E. Zaccarelli, Phys. Rev. Lett. **94**, 195504 (2005).
[15] M. Imai, I. Yoshida, T. Iwaki, and N. Nakaya, J. Chem. Phys. **122**, 044906 (2005).
[16] For a recent application to homopolymer solution see V. Krakoviack, J. P. Hansen, and A. A. Louis, Phys. Rev. E **67**, 041801 (2003).
[17] T. P. Lodge, J. Bang, M. J. Park, and K. Char, Phys. Rev. Lett. **92**, 145501 (2004).